North Atlantic Circulation Regimes and Heat Transport by Synoptic Eddies

PAOLO RUGGIERI, M. CARMEN ALVAREZ-CASTRO, PANOS ATHANASIADIS, ALESSIO BELLUCCI, STEFANO MATERIA, AND SILVIO GUALDI

Centro Euro-Mediterraneo sui Cambiamenti Climatici (CMCC), Bologna, Italy

(Manuscript received 5 July 2019, in final form 8 February 2020)

ABSTRACT

Meridional transport of heat by transient atmospheric eddies is a key component of the energy budget of the middle- and high-latitude regions. The heat flux at relevant frequencies is also part of a dynamical interaction between eddies and mean flow. In this study we investigate how the poleward heat flux by high-frequency atmospheric transient eddies is modulated by North Atlantic weather regimes in reanalysis data. Circulation regimes are estimated via a clustering method, a jet-latitude index, and a blocking index. Heat transport is defined as advection of moist static energy. The focus of the analysis is on synoptic frequencies but results for slightly longer time scales are reported. Results show that the synoptic eddy heat flux is substantially modulated by midlatitude weather regimes on a regional scale in midlatitude and polar regions. In a zonal-mean sense, the phases of the North Atlantic Oscillation do not significantly change the high-latitude synoptic heat flux, whereas Scandinavian blocking and the Atlantic ridge are associated with an intensification. A close relationship between high-latitude (midlatitude) heat flux and Atlantic jet speed (latitude) is found. The relationship between extreme events of synoptic heat flux and circulation regimes is also assessed and reveals contrasting behaviors in the polar regions. The perspective that emerges complements the traditional view of the interaction between synoptic eddies and the extratropical flow and reveals relationships with the high-latitude climate.

1. Introduction

The transport of heat is a fundamental phenomenon in planetary oceans and atmospheres. Transfer of heat from low to high latitudes has an intimate connection with nonuniform insolation, but its partitioning and variability stimulated decades of research and efforts to understand a surprisingly complex phenomenon. Outside of the tropics, a large fraction of heat transport is undertaken by the atmosphere (Czaja and Marshall 2006; Trenberth and Caron 2001). Atmospheric heat transport is often partitioned into a zonal-mean and time-mean component and two eddy components, stationary and transient. The process of development of high-frequency transient synoptic eddies in a baroclinic atmosphere was discussed in the seminal paper by Eady (1949); the presence of strong temperature gradients can sustain the growth of perturbations on time scales typically shorter than 6–9 days, and the net effect of meridional wind and temperature anomalies from a long-term mean is a poleward heat flux. Advection of heat on these scales is also part of an energy exchange between eddies and mean flow, which is well described for the midlatitudes in the context of the baroclinic life cycle (e.g., Simmons and Hoskins 1978), and is organized in two main storm tracks, one in the Pacific and one in the Atlantic. From this perspective, transient eddy heat flux feeds on strong horizontal temperature gradients concentrated in the central and western part of the Atlantic and the Pacific Oceans, and their variability is embedded with shifts of the eddy-driven jet in oceanic sectors.

Low-frequency fluctuations of the midlatitude flow are known to influence the storm tracks (and the eddies) by steering their path (Branstator 1995). On the other hand, an avenue of recent studies (Novak et al. 2015; Straus 2010; Rivière 2009) developed and detailed the idea of synoptic eddy feedbacks on the mean flow

Denotes content that is immediately available upon publication as open access.

Supplemental information related to this paper is available at the Journals Online website: https://doi.org/10.1175/JCLI-D-19-0498.s1.

Corresponding author: Paolo Ruggieri, paolo.ruggieri@cmcc.it

DOI: 10.1175/JCLI-D-19-0498.1

(Hoskins et al. 1983; Mullen 1987). Their results emphasize the importance of pulses of synoptic eddy activity on the low-frequency variability of the atmosphere.

The study of the variability of the transient eddy heat flux in high-latitude regions, poleward of the strong baroclinic zones, apparently followed a parallel research path. The early study of Overland et al. (1996) shows that the region between Greenland and the Barents Sea experiences the strongest eddy heat transport in polar regions and also the largest variability. In Overland et al. (1996) the important role of stationary and transient eddies is analyzed, and the transient component appears to be able to reach remote regions in the polar cap, eventually becoming a dominant component at about 70°–75°N. It was not clear at the time to what extent this transient signal was due to fluctuations in atmospheric temperature and wind associated with large-scale waves, to the propagation of storms into polar regions, or to a secondary storm track with cyclogenesis in the Arctic. The final word on this question is, perhaps, still lacking.

Adams et al. (2000) noted that eddies are fundamental to the horizontal redistribution of heat in the boundaries of the Arctic region. Also, they state that stationary eddies dominate on the Pacific side, whereas transient eddies dominate on the Atlantic side. They found that the Arctic Oscillation (AO) has little impact on the modulation of the eddy heat transport, a result that is rather surprising in view of the impact of the AO on the midlatitude storm track (Nie et al. 2008). More recently, Seierstad et al. (2007) studied how teleconnection patterns explain the variability of the two main storm tracks (Atlantic and Pacific) looking at high-frequency fluctuations of sea level pressure. For the Atlantic they find a dominant role of the NAO, a regional influence in the Labrador Sea by the east Atlantic pattern, and a role of the Scandinavian pattern (and of the east Atlantic/western Russia) over Europe.

The works of Messori and Czaja (2013) and Messori and Czaja (2015) raised awareness of the impulsive and "sporadic" nature of high- and midlatitude transient eddy heat flux (including low frequencies), providing a picture of a highly variable field and noting that a few days can eventually explain most of the heat flux of a season. In particular, Messori and Czaja (2015) suggested a potential association between low-frequency variability of the storm tracks and pulses of eddy heat transport.

Woods et al. (2013) analyzed moisture intrusions into the Arctic during the 1990–2010 period in four sectors, namely, the Labrador Sea, the GIN (Greenland, Iceland, and Norwegian) seas, the Barents–Kara Seas, and the Pacific. They found that the intrusions are favored by a blocking high on the eastern side of the sector and suggested that transport is done by poleward-propagating storms, suggesting an important role of transient eddies also for instantaneous heat flux extremes, in association with a large-scale pattern.

The picture given by the aforementioned studies suggests the following: 1) The transient eddy heat flux is relevant to the energy budget of the pole and the synoptic component has a major poleward extension in the Atlantic region. 2) The variability of transient eddy heat flux embodies a two-way interaction with the low-frequency variability of the atmosphere. In the Atlantic it is largely ascribable to the alternating phases of the NAO, or more generally north–south shifts of the jet, but no clear evidence is found of any modulation (by the NAO) of high-latitude transient eddy heat flux. 3) There is emerging and growing evidence of impulsive and regional injections of heat and moisture into the Arctic. This phenomenon involves multiple scales and frequencies but shows a link with the large-scale circulation of the atmosphere and with poleward propagation of storms.

In this study, we investigate the modulation of transient eddy atmospheric heat flux by low-frequency variability of the atmospheric circulation in the North Atlantic sector. Heat transport is defined by meridional advection of moist static energy, and the circulation anomalies are diagnosed with a widely used clustering technique, a jet-latitude index, and a blocking index. The analysis of the high-frequency (synoptic) component of the flux is complemented with specific aspects of the corresponding low-frequency and total heat flux. Along the lines of the three points highlighted previously, the analysis presented in this study can associate certain flow regimes with the climatological extension of the eddy heat flux into the Nordic seas (shown later in this document). Moreover, specific features of wave–mean flow interaction can be discussed in view of the presented results. Finally, insights from our results can clarify how extremes of high-frequency flux develop given a flow regime. Indications on how these extremes relate to the total instantaneous heat flux are given.

The analysis is carried out for the extratropics in the Northern Hemisphere and results are based on an atmospheric reanalysis for a total of 38 extended cold seasons.

Establishing quantitative relationships between circulation regimes and poleward heat transport by transient eddies can help understand linkages between midlatitudes and the Arctic, and evaluate how they are represented in coupled GCMs. After this introduction, in section 2 we describe methodology and data used, in section 3 an observational analysis is presented, and in section 4 we discuss findings, implications, and applications that are summarized in section 5.

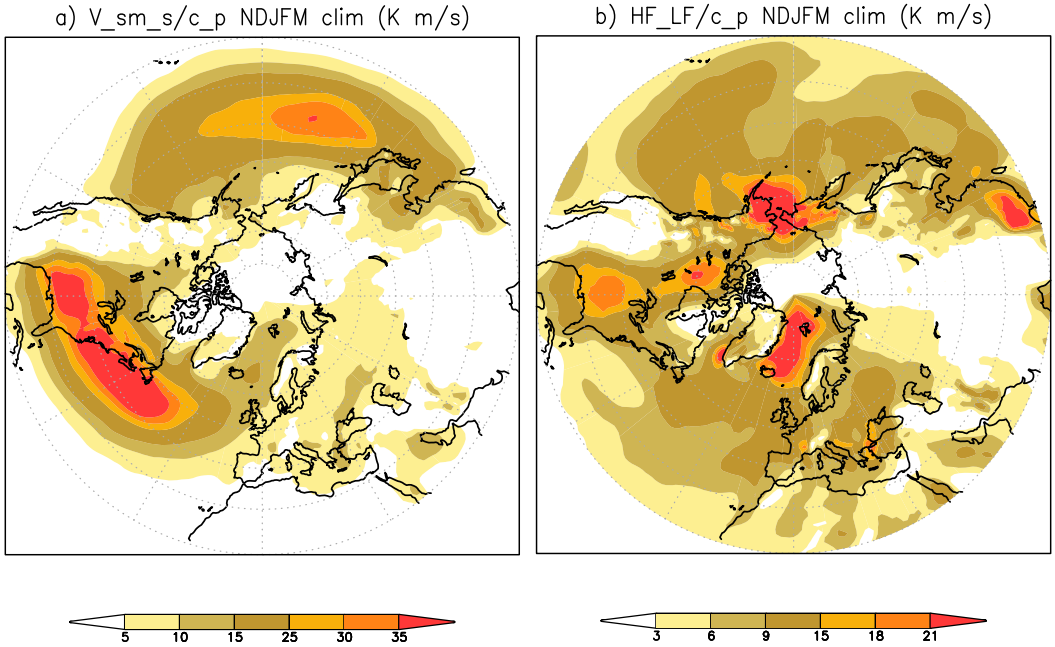

FIG. 1. (a) Climatology of synoptic eddy heat flux (SEHF; defined as $V_s m_s / c_p$; K m s^{-1}) at 850 hPa for NDJFM, 1980–2017. (b) As in (a), but for the low-frequency heat flux (HF_{LF}; defined as $V_L m_L + V_L m_s + V_s m_L$). See text in section 2 for details about the computation of the heat flux.

2. Methodology

a. Data

For this study, 6-hourly data from ERA-Interim (Dee et al. 2011) are obtained on a 1° × 1° regular longitude–latitude grid on selected pressure levels (100, 200, 300, 400, 500, 600, 700, 775, 850, and 925 hPa). Data used include geopotential height (Z), zonal (U) and meridional (V) components of wind, air temperature (T), and specific humidity (Q). Circulation indices introduced in the following section are computed on a daily mean basis.

b. Circulation regimes

The presented analysis is based on three different approaches to identify patterns of low-frequency variability in the Atlantic sector, namely weather regimes, the jet-latitude (and speed) index, and a blocking index (Fig. 1).

Weather regimes have been computed following the method of Michelangeli et al. (1995) and Yiou et al. (2008). The 10 leading empirical orthogonal functions of Z at 500 hPa and the corresponding principal components are computed. Then a k-means algorithm is applied to daily data across the 1979–2017 extended cold seasons [November–March (NDJFM)], with the choice of four weather regimes over the North Atlantic region (20°–70°N, 80°W–50°E). Daily data classifications are obtained by determining the minimum of the Euclidean distances to the four weather regime centroids. Generally, the winter atmospheric circulation in the North Atlantic sector is classified into four weather regimes (Michelangeli et al. 1995; Kimoto and Ghil 1993a,b; Corti et al. 1999). Indeed, Michelangeli et al. (1995) have computed a classifiability index $c^*(k)$, where k is the number of clusters, in order to determine the optimal number of regimes varying from $k = 2$ to $k = 10$. After $k = 5$ the index lies within the noise confidence interval, meaning that North Atlantic data are not more classifiable than data coming from a multinormal distribution.

A jet-latitude index (JLI) has been defined following the rationale of Woollings et al. (2010): U at 850 hPa is averaged zonally in the sector 15°–75°N, 60°W–0° and the resulting wind profile is low-pass filtered with a 10-day running mean. Then, the jet speed is defined as the maximum wind value and the jet latitude is defined as the corresponding jet latitude.

A blocking index is computed following Scherrer et al. (2006) and it is an extension of the blocking detection method introduced in Tibaldi and Molteni (1990), based on reversal of the meridional gradient of geopotential height at 500 hPa. For each latitude ϕ_0 between 30° and 75°N, the longitudes where $[Z(\phi_0) - Z(\phi_0 - \Delta\phi)]/\Delta\phi > 0$ and $[Z(\phi_0 + \Delta\phi) - Z(\phi_0)]/\Delta\phi < 10\,\text{m}\ (1^\circ\ \text{lat})^{-1}$ are considered blocked. Here Z is the geopotential height at 500 hPa and $\Delta\phi = 15°$.

c. Definition of transient heat flux

In this study the focus is on the variability of the transient eddy heat flux defined as the product of the high-frequency component of meridional velocity and moist static energy (Fig. 2). Moist static energy is defined as $m = c_pT + L_vQ + \Phi$, where c_p is the specific heat of dry air at constant pressure, L_v is the latent heat of vaporization at a reference temperature, and Φ is the geopotential. Values of constants used in the computation are $c_p = 1004\,\mathrm{J\,K^{-1}\,kg^{-1}}$ and $L_v = 2.51 \times 10^6\,\mathrm{J\,kg^{-1}}$. The physical interpretation of m is widely discussed in literature (e.g., Peixoto and Oort 1992; Holton 1973) and the transport of heat expressed as advection of m is established and discussed by, for example, Liang et al. (2018). The flux is diagnosed on all pressure levels used in the study, but the 850-hPa level is often used as a reference for the whole tropospheric column.

Transient eddy quantities on synoptic frequencies (named hereafter V_s for velocity and m_s for moist static energy) are defined as the deviation from a 9-day running mean. Sensitivities to the choice of the frequency decomposition method have been conducted for a large portion the presented material and results are found to be only quantitatively affected by the choice of the filtering method. Synoptic eddy heat flux (SEHF) is defined as V_sm_s. Composites of instantaneous V_sm_s on circulation regimes are shown in Figs. 3–11. Selected analyses for a filtered heat flux $\overline{V_sm_s}$ such that $\overline{V_s} = \overline{m_s} = 0$ are presented in Figs S1 and S2 in the online supplemental material and do not show qualitative differences from the corresponding analysis of the instantaneous heat flux.

Zonal means are used as a measure of the heat flux at the lower boundary of the corresponding polar cap (i.e., the cap bounded by the reference latitude), but they are also representative of the local signal detected in the Euro-Atlantic sector.

The analysis has been complemented with low-frequency components and with the vertically integrated total heat flux. A low-frequency component of velocity V_L and temperature T_L is defined as a residual: for example, $V_L = V - V_C - V_S$, where V_C is a time-mean field and V_S is the previously defined synoptic component. Intermediate frequency bands (see Figs. 12 and 13) are computed by filtering daily data with the bandpass function of the Climate Data Operators tool (Schulzweida et al. 2019). The vertical integral of total heat flux used in Table 1 is computed using pressure levels between 100 and 925 hPa; the integral is estimated numerically with the trapezoidal rule. It is recalled here that the relationship between instantaneous total and transient heat flux is such that $Vm = V'm' + V'm_C + V_Cm' + V_Cm_C$, where $V' = V_s + V_L$ and $m' = m_s + m_L$.

Statistical significance is assessed using an unpaired Student's t test with a number of effective degrees of freedom that accounts for the autocorrelation of time series and with a bootstrap method. The bootstrap method (see Fig. 5) is based on sampling with replacement of blocks of consecutive days with jet latitude (or speed) falling in the same interval.

Anomalies of heat flux are computed by subtracting from the daily mean value the corresponding daily climatology. The daily climatology is computed by averaging the 38 values corresponding to the years in the analysis period.

3. Results

Synoptic storm activity is mainly detected in the two tracks in correspondence of the Atlantic and Pacific Oceans, as shown by Fig. 1a. The poleward heat flux is broadly coincident with the low-level transient eddy kinetic energy (not shown). There is a noticeable poleward extension of the heat flux into the Nordic and Barents Seas that reaches higher values and latitudes than the heat flux in the Bering Strait. For slower eddies (in Fig. 1b) local maxima can be found in the midlatitude band but there are two noticeable peaks in polar regions, one in the Nordic seas and one in the Bering Strait. The field shown in Fig. 1b is dominated by V_Lm_L but all terms are used for completeness. The analysis of this component of the low-frequency flux is aimed at understanding if Atlantic weather regimes modulate the extension in the Nordic seas, where its magnitude is larger than the synoptic counterpart.

Figures 2a–d show the four weather regimes identified in NDJFM 1979–2017. In this manuscript they are named Scandinavian blocking (Scand; Fig. 2a), Atlantic ridge (Ridge; Fig. 2b), positive NAO (NAO+; Fig. 2c), and negative NAO (NAO−; Fig. 2d). Three of these regimes feature a positive, blocking-like geopotential height anomaly in the northern part of the domain, with the exception of NAO+.

The distribution of jet latitude and speed are shown in Figs. 2e and 2f: as documented in Woollings et al. (2010) for DJF, the JLI has a trimodal distribution and Fig. 2e shows that the trimodality is conserved if the extended cold season is used. It is possible to identify a southern peak with a low-level jet at about 35°N, a central peak at about 45°N, and a northern peak at 55°N. The two tails of the distribution are noticeable; in particular, the jet can be detected at very high latitudes between 60° and 70°N. The jet speed shows a unimodal distribution centered at about $12.5\,\mathrm{m\,s^{-1}}$ and ranging from 2.5 to $22.5\,\mathrm{m\,s^{-1}}$.

The correspondence between weather regimes and JLI has been analyzed by Madonna et al. (2017). The

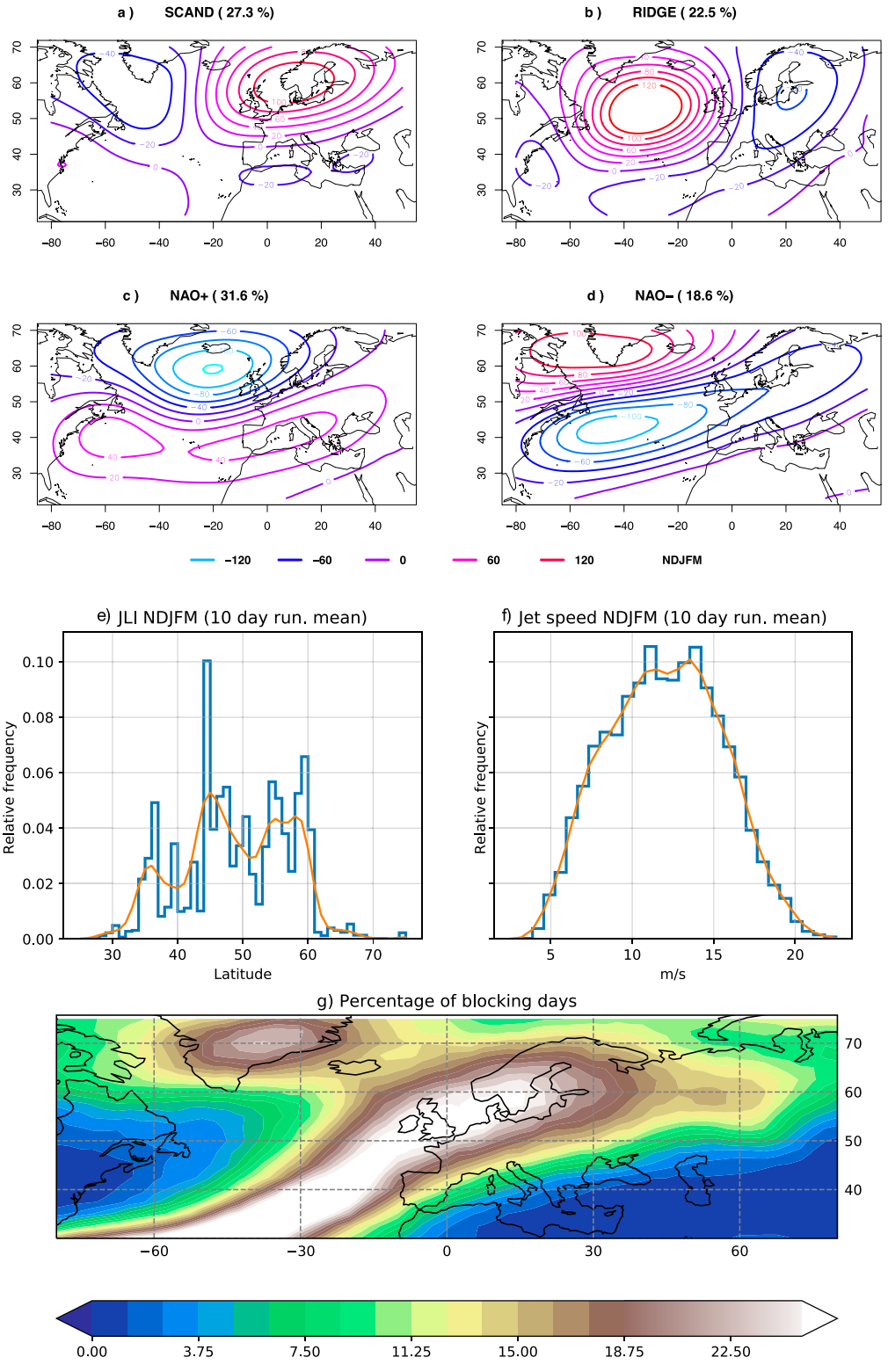

FIG. 2. The four North Atlantic weather regimes, jet-latitude/speed index, and the blocking index, for the extended cold season in ERA-Interim. (a) Scand, (b) Ridge, (c), NAO+, and (d) NAO−. Contours indicate anomalies of geopotential height at 500 hPa (m). The number shown in parentheses in each panel title is the percentage of days corresponding to the regime. (e) Smooth probability density function and histogram of relative frequency of the jet-latitude index. (f) As in (e), but for the jet speed. (g) Percentage of blocked days based on reversal of the geopotential height meridional gradient.

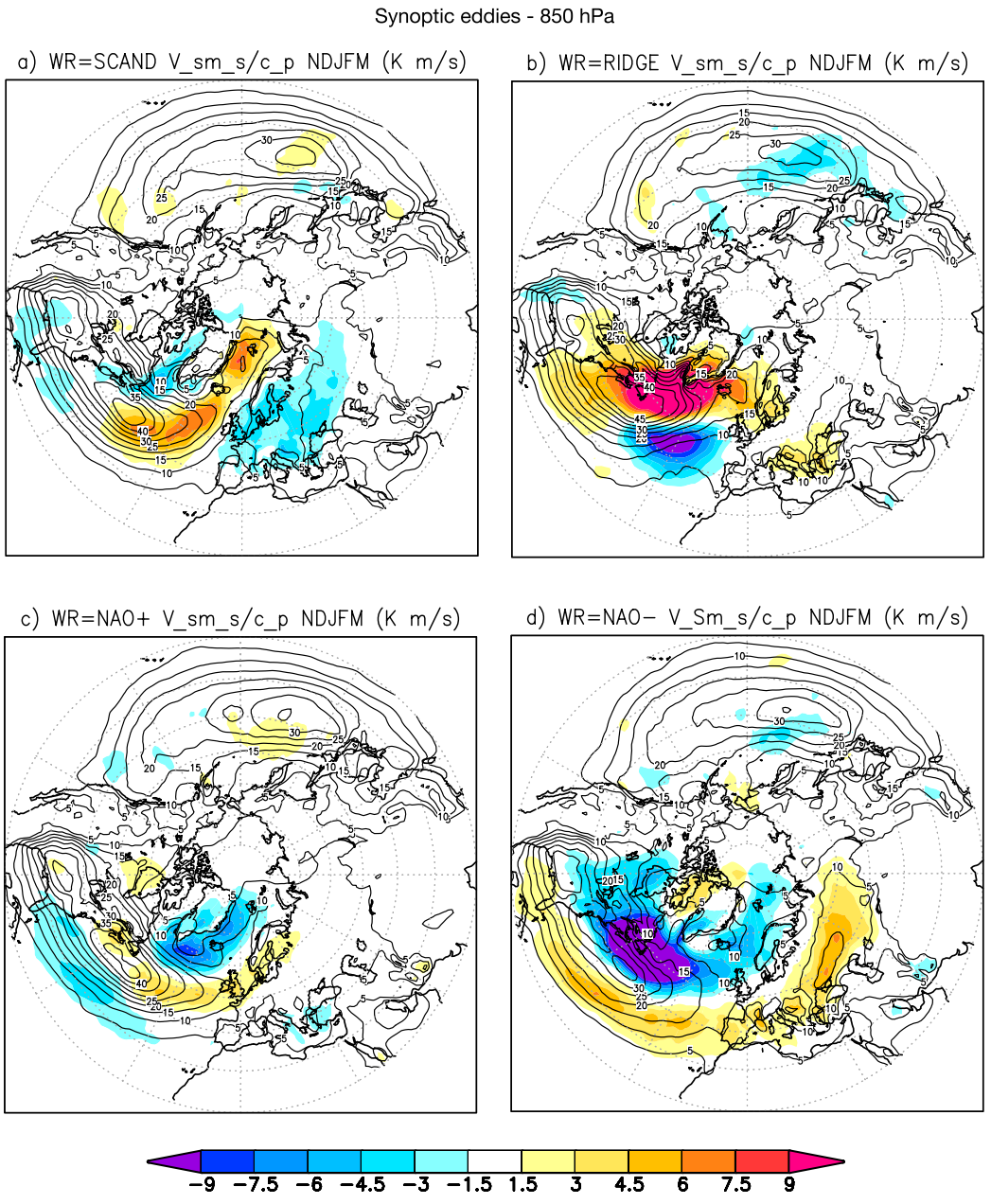

FIG. 3. Composites of anomalies (shading) of meridional moist static energy flux by synoptic eddies ($V_s m_s$; K m s^{-1}) for the four weather regimes. Anomalies are computed from a daily climatology. Contours indicate the mean field associated with the weather regime, obtained by adding the anomalies and the mean NDFJM value.

southern regime of the JLI corresponds broadly to the NAO− and the central one to the NAO+, the Ridge is associated with the northern regime, and Scand is found to be linked with a "mixed" jet regime that spans all jet latitudes, although northern latitudes are found to be more likely. The JLI can therefore complement and detail the picture offered by weather regimes and establish a relationship between SEHF and specific features of the Atlantic jet.

Finally, Fig. 2g shows the climatological blocking frequency, defined as the percentage of days with a blocked grid point. Noticeable features are a local maximum over Greenland and a band over Europe. A detailed description of the index and a comparison with other methodologies can be found in Scherrer et al. (2006). The relationship between blocking and JLI is examined by Woollings et al. (2010): Greenland blocking is associated with the southern regime of the jet,

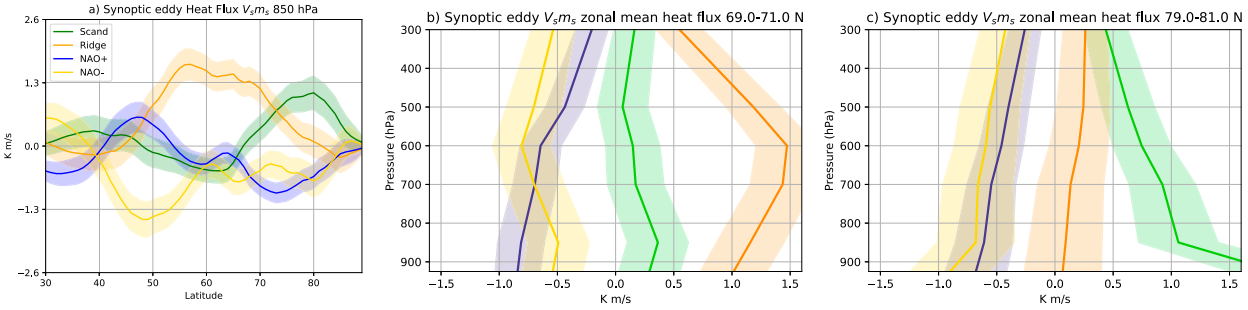

FIG. 4. Profiles of meridional moist static energy flux by transient synoptic eddies ($V_s m_s$; K m s^{-1}) for the four weather regimes. (a) Zonal mean of anomalies at 850 hPa. (b) Vertical profile of anomalies between 69° and 71°N, sampled at 300, 500, 600, 700, 850, and 925 hPa. (c) As in (b), but between 79° and 81°N. Shading indicates the 99% confidence interval according to an unpaired *t* test.

while Scandinavian blocking is not strongly related to a preferred jet latitude, but is more frequent during the northern jet regime. The combination of results presented by Madonna et al. (2017) and Woollings et al. (2010) indicates that Greenland blocking is typically associated with the NAO−, while Scandinavian blocking is more frequent during the Scand regime. An overview of different definitions of circulation regimes in the Northern Hemisphere can be found in Hannachi et al. (2017).

The link between the circulation regimes, defined with the three different methods introduced previously, and the heat flux is examined in the subsequent sections.

a. *Synoptic eddy heat flux and Atlantic weather regimes*

In Fig. 3, the relationship between the low-level synoptic eddy heat flux and the Atlantic weather regimes is shown. In this figure, anomalies of $V_s m_s$ are composited for days classified with a selected weather regime. It can be seen in Fig. 3a that Scandinavian blocking implies stronger flux in the central Atlantic, in the core of the jet, and weaker transport in continental Europe. Between 30°W and 30°E, the storm track is deflected poleward, resulting in a particularly strong flux in the GIN and Barents Seas. The Atlantic Ridge (Fig. 3b) induces a north–south dipole in the central Atlantic, with intensified transport in the Labrador Sea, Denmark Strait, and northern Europe. During the positive phase of the NAO (Fig. 3c) transport is intensified in the core of the jet and weakened on the poleward and equatorward sides. This fact is consistent with a strong jet acting as a meridionally confined waveguide. Finally, the negative phase of the NAO (Fig. 3d) shows a suppression of the heat flux in the upstream region of the Atlantic jet and a moderate equatorward shift, with a positive signal found over Eurasia. The asymmetry between the NAO+ and NAO− is noticeable, particularly for the northwestern Atlantic region.

The zonal mean of the fields shown with shadings in Fig. 3 is shown in Fig. 4a. The Ridge features a strong intensification of the flux centered at about 60°N, with a modest reduction at lower latitudes. Scand shows a similar feature but shifted north by 15°–20°, with the positive peak centered around 80°N. NAO+ is generally the closest to climatological conditions, being the most frequent regime, and is characterized by a positive peak in the midlatitudes, and a relatively strong suppression in the polar cap. NAO− corresponds to a negative peak in the midlatitudes, but remarkably it is associated with a reduction in polar regions, where it is not clearly distinguishable from the NAO+. Considering 70°N as reference latitude, in Fig. 4b, and using the NAO+ and NAO− as a baseline with low flux, the role of the Ridge stands out as the regime with the largest heat flux on the boundary of the polar cap. Looking farther north, in Fig. 4c, the Scandinavian pattern shows the largest values, indicating an important role of this regime for heat redistribution between the low Arctic and high Arctic by transient synoptic eddies.

Figures 4b and 4c also show that the signal sampled at 850 hPa is representative of the variability of the vertically integrated heat flux for synoptic eddies and confirm the similarity of the phases of the NAO in polar regions.

b. *Synoptic eddy heat flux and jet latitude and speed*

The relationship between jet latitude and speed and zonal-mean SEHF is explored in Fig. 5. These plots are constructed by "binning" the value of the zonal-mean SEHF at a reference latitude as a function of the speed (left panels) and latitude (right panels) of the jet. The synoptic heat flux is sampled at four reference latitudes between 50° and 80°N, and at 850 hPa. Looking at polar latitudes (Figs. 5a–f), between 60° and 80°N, it can be seen that the heat flux and the jet speed are anticorrelated; a strong jet implies weak poleward transport by synoptic eddies on the boundary and within the polar

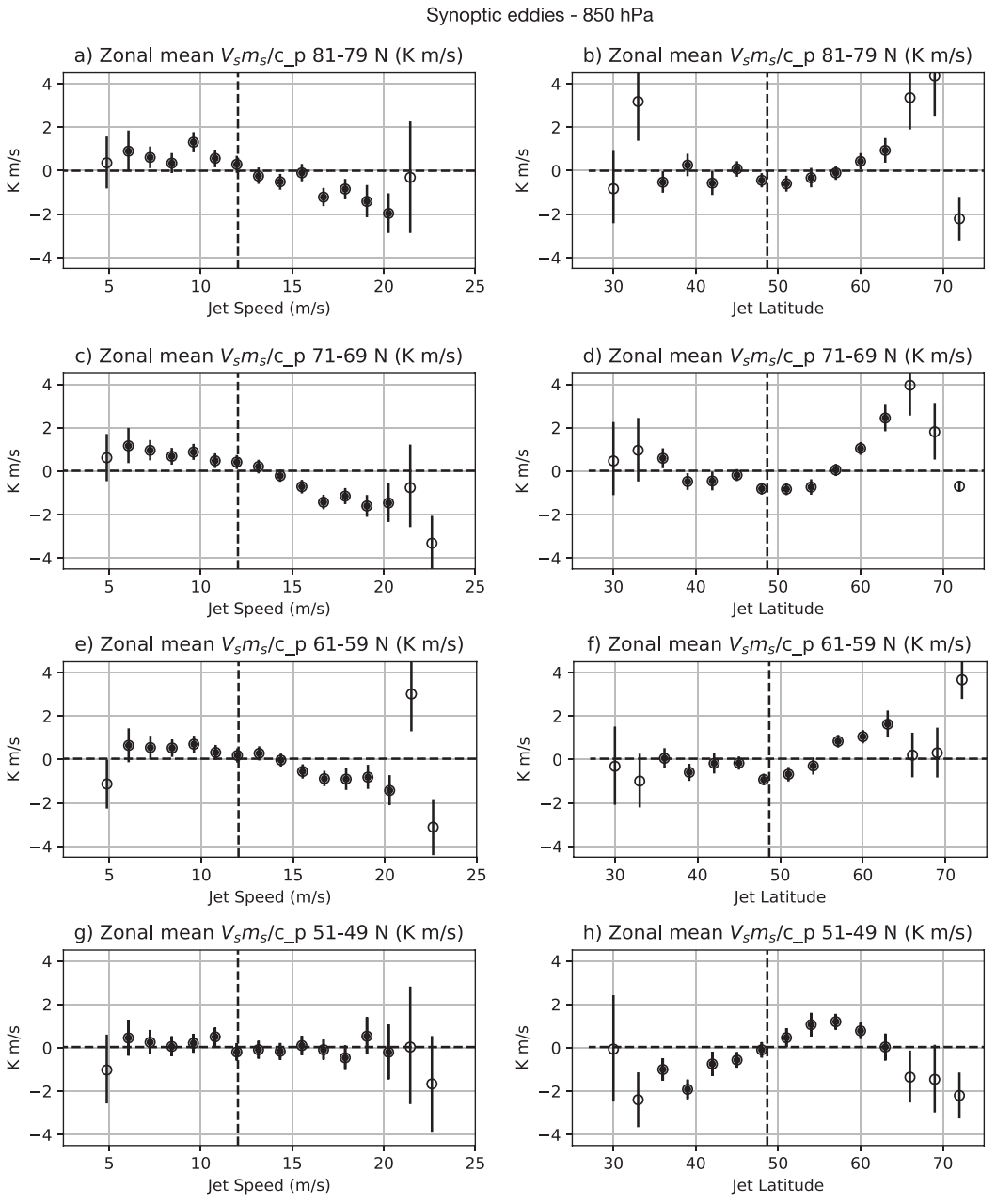

FIG. 5. Relationship between zonal-mean synoptic eddy heat flux at four reference latitudes and (left) jet speed and (right) latitude in the North Atlantic. Latitudes used are (a),(b) 80°, (c),(d) 70°, (e),(f) 60°, and (g),(h) 50°N. Error bars indicate a 99% confidence interval estimated with a bootstrap method. Empty circles indicate that the value corresponds to less than 1% of days. A dashed horizontal line marks the zero value; a dashed vertical line marks the mean jet latitude or speed.

cap and vice versa. The dependency on the jet latitude is more complex (Figs. 5b,d,f). The central jet regime is associated with the lowest values of heat flux. When the jet is in the southern regime, the value of the heat flux is higher than the central one, but slightly lower than the climatological mean, as indicated by the negative anomaly. When the jet is poleward of 50°N, the flux in polar regions increases linearly with the latitude of the jet, reaching particularly high values when the jet latitude is greater than 60°N. Note that such extreme poleward excursions of the jet are fairly infrequent, as indicated by the PDF of the JLI in Fig. 2e. More

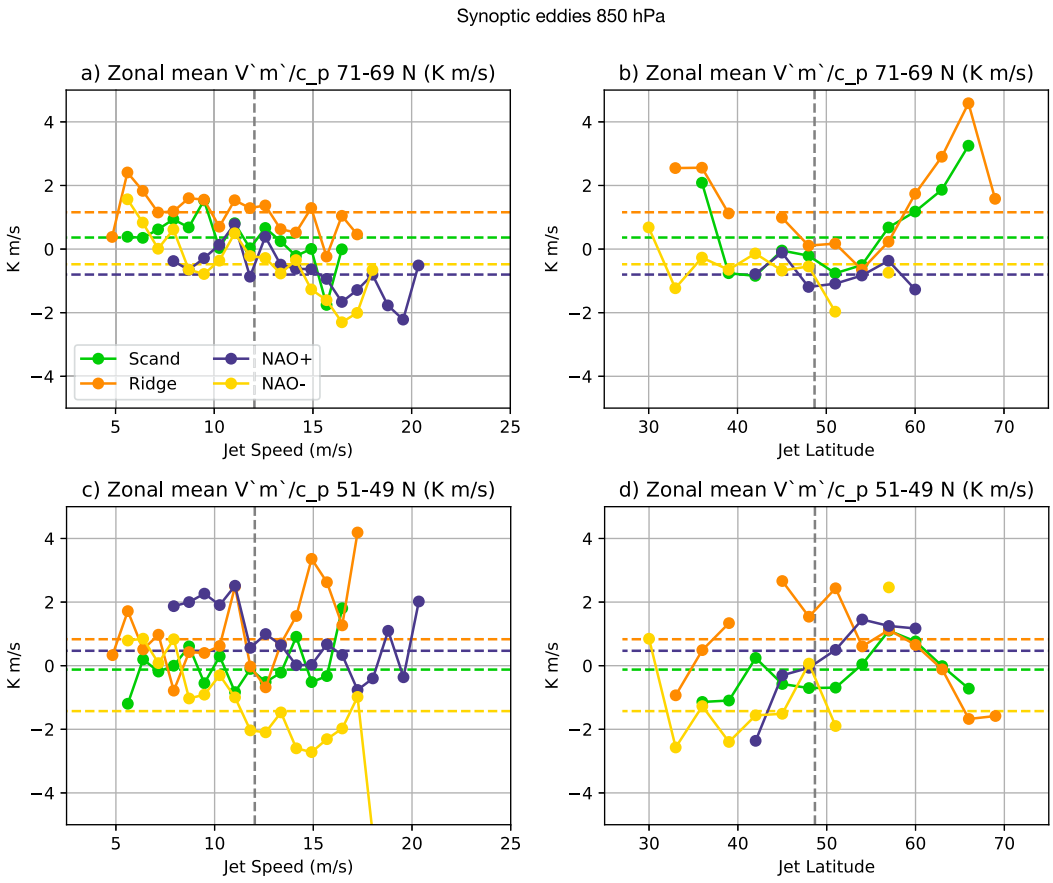

FIG. 6. As in Fig. 5, but for the four weather regimes separately. Points corresponding to less than 1% of days are not displayed. The dashed horizontal lines indicate the mean anomaly for the corresponding weather regimes. A dashed vertical line marks the mean jet latitude or speed.

precisely, events (days) with JLI $\geq 60°$N are about 6.5% of the total, while up to 25% have JLI $> 55°$.

In the midlatitudes (50°N; Figs. 5g,h), SEHF is almost insensitive to variations of the jet speed around its climatological value, but sensitivity is larger on the tails, where sampling uncertainty is also large. The relationship with the jet latitude resembles a concave parabola, with its maximum centered around 55°N (i.e., a jet displaced northward with respect to the mean latitude). This optimal latitude is found also if slightly different definitions of the JLI are used and if any latitude between 45° and 55°N is used for the zonal-mean SEHF (not shown). The heat flux is substantially reduced for an equatorward displaced jet, and it increases almost linearly with jet latitude up to 55°N, where it starts decreasing, being smaller than average for extreme poleward displacements. SEHF in midlatitudes depends weakly on jet speed and strongly on jet latitude, and, if extreme states of the jet are not considered, then SEHF increases linearly with jet latitude. Assuming that variations in the transport detected here are due mostly, if not only, to changes in the Atlantic sector (and Fig. 3 is reassuring in these respects), then the picture is consistent with the results of Novak et al. (2015) [see, e.g., Fig. 6 in Novak et al. (2015)].

A useful exercise is to repeat the binning method in Fig. 5 retaining only days with a weather regime in common. This analysis is shown in Fig. 6. Starting again from the polar cap, we see that the linear relationship between jet speed and SEHF is conserved also for the individual regimes, and that both the jet speed and the weather regimes together set the value of the heat flux. There is no dependence on the jet latitude for the NAO±. The aforementioned extremes on the poleward tail of the JLI are notably explained only by the Atlantic ridge and the Scandinavian blocking.

Looking at the midlatitudes, we see that there is no systematic dependence on the jet speed. The NAO− produces the largest negative excursion, while the largest positive values depend on the exact choice of the reference latitude but are attributable to Ridge and

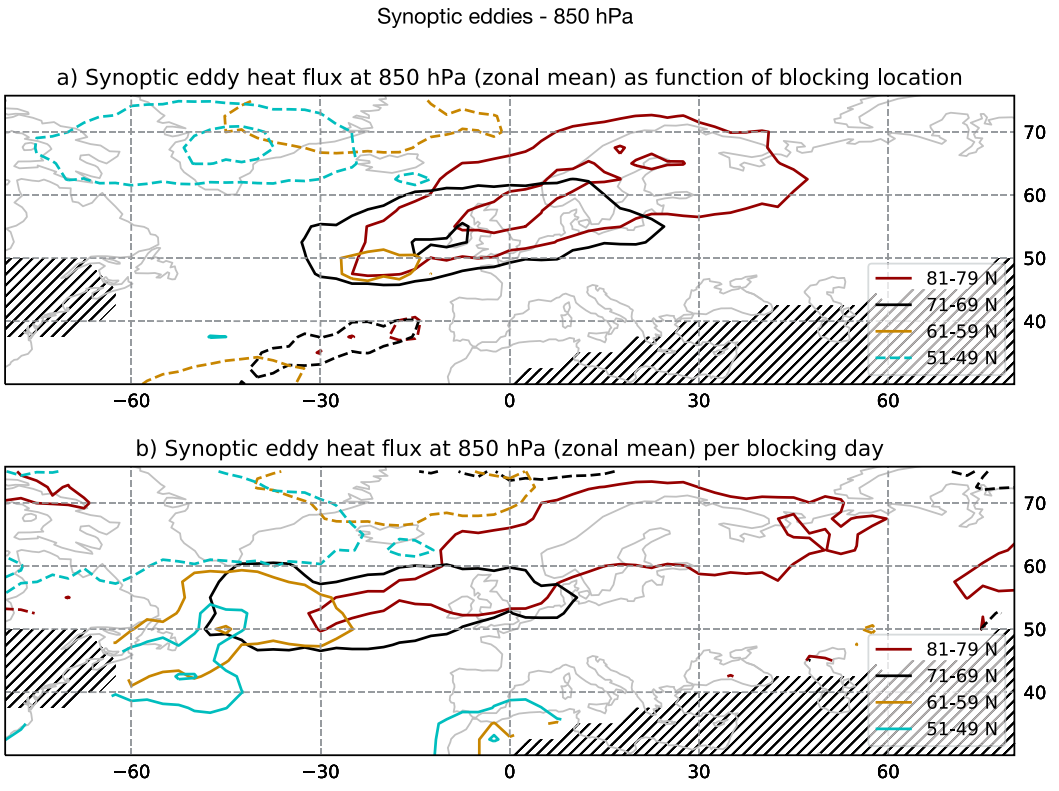

FIG. 7. Zonal-mean SEHF at 850 hPa associated with occurrence of blocking. Blocking days are detected with a 2D blocking index based on the reversal of the geopotential height gradient at 500 hPa. The displayed field is obtained taking the sum of the zonal-mean synoptic SEHF at four reference latitudes (50°, 60°, 70°, and 80°N) when blocking is detected at the corresponding grid point. (a) The field is divided by a factor of 170 days. (b) The resulting 2D field is divided by the number of blocked days and thus shows the anomalous SEHF per "blocking day." In both panels contours are drawn at ± 2 and ± 4 K m s^{-1} day^{-1}. Hatched areas correspond to regions with climatological blocking frequency less than 1%.

NAO+. There is evidence of a compensation of signals between the NAO− and the Ridge. The relationship found in Fig. 5h for midlatitude heat flux on jet latitude is conserved for individual regimes (Fig. 6d).

The comparison of these results with the analysis of the weather regimes presented in the previous sections is insightful. Let us use Fig. 5h as representative of the covariability of midlatitude heat flux and Atlantic eddy-

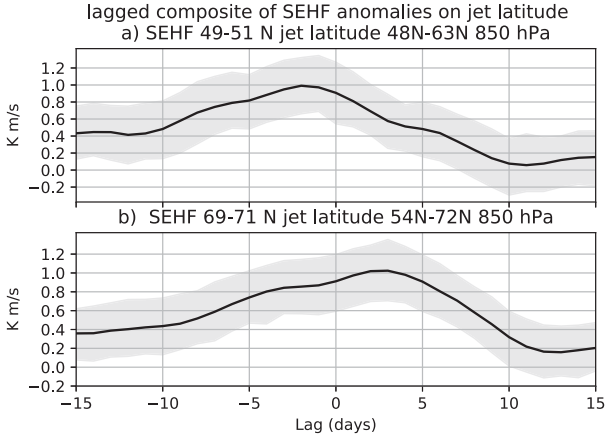

FIG. 8. Lead–lag composite of SEHF at 50°N composited for days with jet latitude between 48° and 63°N. (b) As in (a), but for SEHF at 70°N composited for days with jet latitude between 54° and 72°N. Shading indicates a 99% confidence interval.

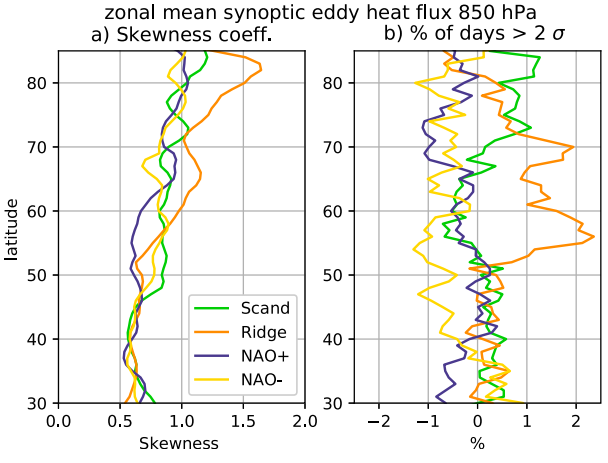

FIG. 9. (a) Latitudinal profile of the skewness coefficient of the SEHF distribution for the four weather regimes. (b) Percentage of days with SEHF greater than two standard deviations for the four weather regimes.

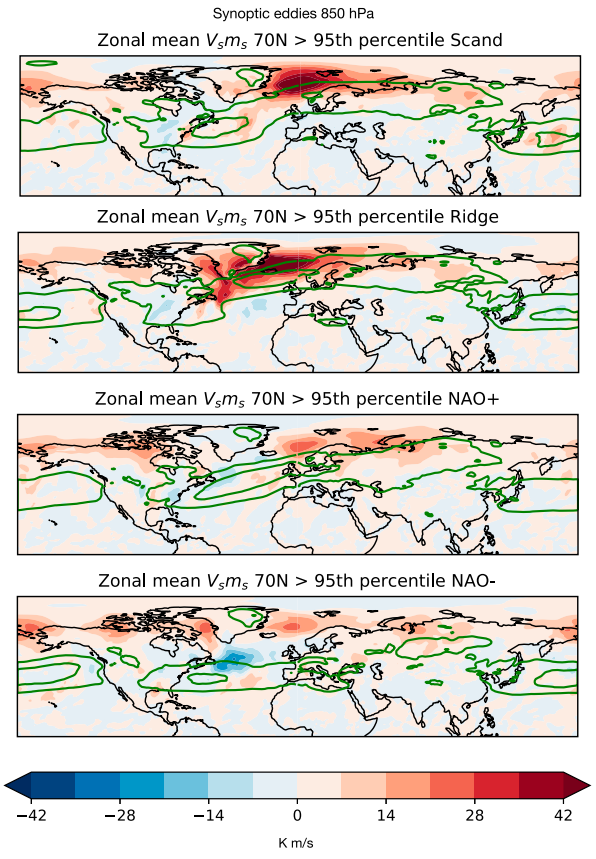

FIG. 10. Composites of anomalous meridional heat transport (shading) for days with extremely positive zonal-mean heat flux at 70°N (>95th percentile), conditional on the occurrence of a weather regime. The corresponding zonal wind field at 850 hPa is shown with green contours. The threshold of the 95th percentile is defined for each regime separately and days above the threshold all belong to the same weather regime.

driven jet and Fig. 5d for the polar heat flux. Comparing them with Fig. 4a, it can be seen that the heat flux sampled at 50°N grows from NAO− (a regime with a jet latitude preferably between 30° and 40°N) to NAO+ (with a jet latitude between 40° and 50°N) and to Ridge (a jet latitude between 50° and 60°N), broadly in agreement with Fig. 5h. Considering now Fig. 4a, at 70°N, we see the weak modulation by the NAO is consistent with the weak changes for jet latitude varying between 30° and 50°N. On the other hand, Scand and Ridge are the two regimes that can be found with a very high jet latitude (see Fig. 6b) and they explain most if not all of the increase of polar heat flux found for a jet latitude greater than 55°N.

The midlatitude heat flux depends strongly on jet latitude even if individual regimes are considered. The same applies to high-latitude heat flux and jet speed, whereas the dependence on jet latitude is dominated by extreme states associated with Scand and Ridge. Many features shown for weather regimes can be reconciled with the analysis of the jet. To some extent the dependence of the heat flux on jet latitude and speed does not depend on the regimes. Some important details emerge, including the dependence of the high-latitude heat flux on the jet speed common to all regimes (Fig. 6a) and the role of extreme jet latitudes attributable to Scand and Ridge (Fig. 6b). It is important to note that Figs. 5 and 6 do not include any information on the frequency of occurrence associated with displayed values. These considerations suggest an interesting role for blocking (discussed in the following section) and for extremes (treated in section 3d).

c. *Synoptic eddy heat flux and Euro-Atlantic blocking*

To investigate the association between blocking in the Atlantic sector and SEHF, in Fig. 7 we show a longitude–latitude map of the anomalous zonal-mean SEHF at selected latitudes in days with blocking detected at a given geographical location. Figure 7a indicates the heat amount transported cumulatively by all days in which blocking is detected at a given geographical location. This quantity can be useful for a comparison with the weather regimes analysis as it scales with the number of blocking days and thus prefers regions where blocking is more recurrent. It can be seen that Greenland blocking suppresses the midlatitude flux, whereas blocking in the eastern Atlantic and Scandinavia intensifies the flux respectively at higher latitudes. Figure 7b indicates instead the average anomalous heat transport "per blocking day." This field can be viewed as a map of SEHF "efficiency" associated with blocking occurring at a certain geographical location. An interesting picture emerges: the occurrence of blocking in the upstream region has implications for the midlatitudes and high-latitude (low-latitude) blocking is associated with negative (positive) anomalies. Blocking in the downstream region (i.e., northern Europe) instead enhances the high-latitude flux. It is possible to draw a zero line from the coast of North America to the Norwegian Sea, following the tilt of the Atlantic jet. Blocking on the poleward side of the line is associated with a reduction of heat flux at a relevant latitude; blocking on the equatorward side produces the opposite effect. Depending on the longitude, the heat flux is modulated predominantly in middle or high latitudes. The behavior described above is peculiar to the North Atlantic and outlines a variegated wave–mean flow interaction if compared to the Pacific (see Fig. S4).

The consistency between the analysis of blocking and that of weather regimes can be visualized comparing the location of positive, blocking-like anomalies in Figs. 2a–d

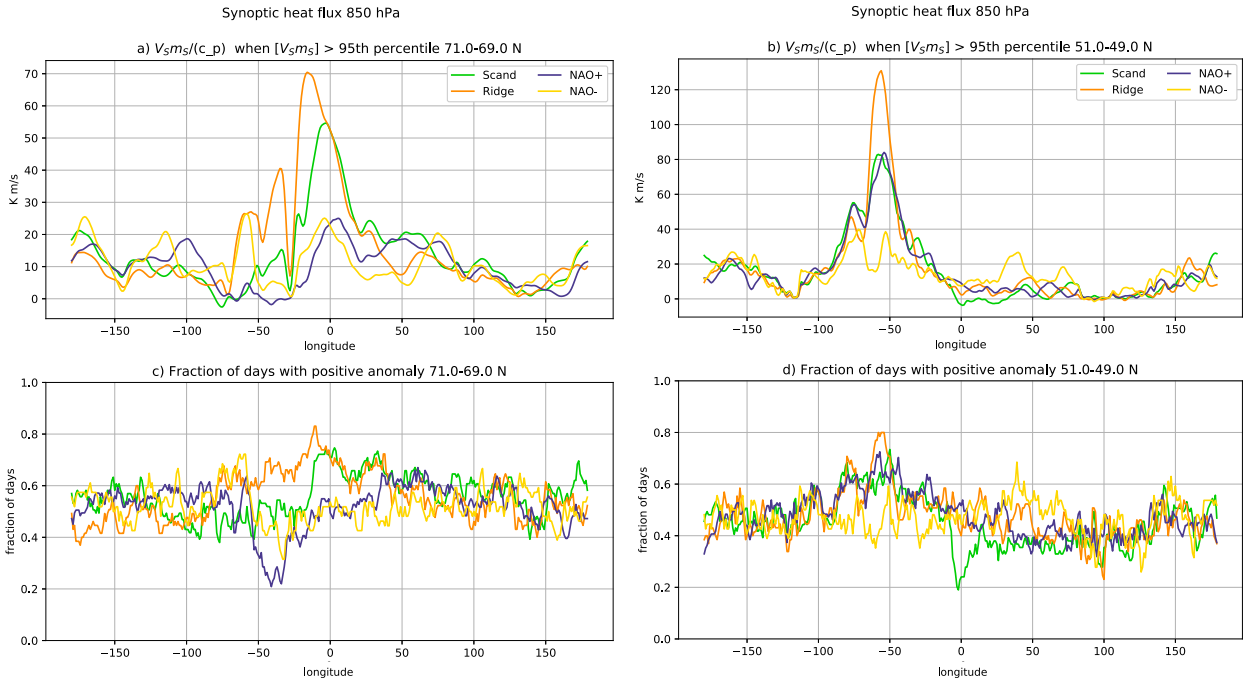

FIG. 11. (a) Composites of anomalous meridional heat transport for days with extremely positive zonal-mean heat flux between 69° and 71°N (>95th percentile), conditional on the occurrence of a weather regime. The threshold of the 95th percentile is defined for each regime separately and days above the threshold all belong to the same weather regime. (b) As in (a), but between 49° and 51°N. (c) Longitudinal profile of fraction of days with positive local heat transport, averaged between 69° and 71°N, in the subset of extremely positive heat transport introduced in Fig. 10a. (d) As in (c), but between 49° and 51°N.

and the corresponding value of the heat flux shown by Fig. 7. The comparison with jet latitude shows an interesting detail that is examined in Fig. 8. Here we see that strong midlatitude SEHF peaks on average at negative lags, whereas the maximum anomaly of the high-latitude component follows days in the northern jet regime. This result highlights the contrasting nature of polar and midlatitudes eddy heat flux variability on the examined time scale and adds nuances to the picture given by Fig. 7. On one hand, pulses of energy transfer to the eddies in the main baroclinic region (west Atlantic around 50°N), on average preceding the poleward displaced jet. On the other hand, downstream and at higher latitudes, the established "blocked" circulation favors the poleward propagation of storms (see also Figs. 5c and 5d). This perspective is further discussed in section 4.

d. Synoptic heat flux extremes

Extremes constitute an important component of the extratropical heat flux by transient eddies and a large fraction of the heat transport is attributable to few, extreme events (Messori and Czaja 2013). The skewness of the atmospheric heat flux in the extratropics is also discussed by Watt-Meyer and Kushner (2018). It is therefore useful to investigate whether the properties of the mean of the distribution discussed in previous sections are common also to the tail of the distribution associated with extremely strong heat flux.

The skewness of the distribution of zonally averaged SEHF as a function of latitude is displayed in Fig. 9. It can be noticed that SEHF has a positively skewed distribution for all individual regimes and the skewness of the distribution increases substantially with latitude

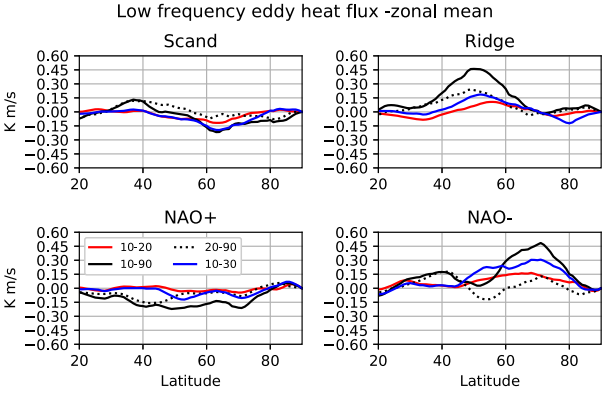

FIG. 12. Zonal mean of the covariance of V and m bandpass filtered in the following ranges: 10–90 (black solid line), 10–30 (blue solid line), 10–20 (red solid line), and 20–90 (black dotted line) days.

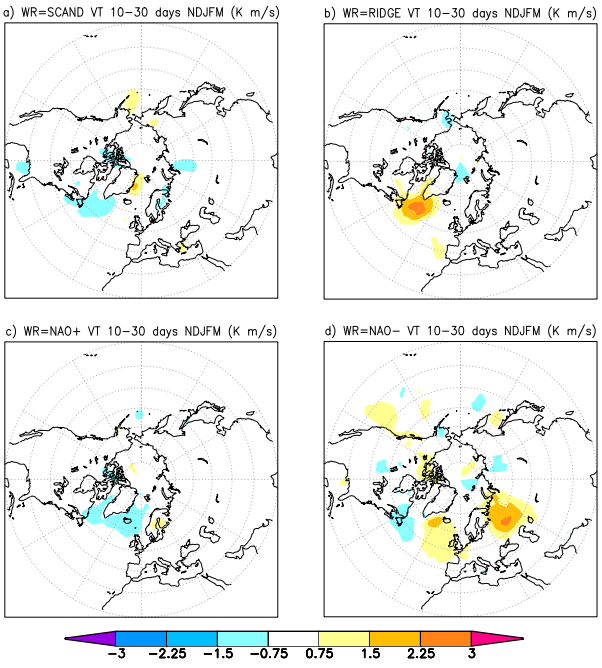

FIG. 13. Composite of the covariance of V and m bandpass filtered in the range of 10–30 days for the four weather regimes.

(Fig. 9a). The Ridge regime is the only one clearly distinguishable from the others and it shows a larger skewness in polar and subpolar regions. The fraction of days with SEHF anomalies larger than two standard deviations (shown in Fig. 9b) suggests that the relative importance of extremely positive heat flux during Scand and Ridge is higher compared to the NAO±.

The analysis presented in Fig. 10 confirms the peculiar role of Scand and Ridge in terms of the spatial structure of extreme zonal-mean heat transport. In this figure, the 95th percentile of zonal-mean synoptic SEHF is computed for the four PDFs associated with individual weather regimes (i.e., the distribution obtained if only days with the selected regime are retained). The SEHF is then averaged for all days above the 95th percentile belonging to the selected weather regimes. The associated 850-hPa zonal wind field is shown with green contours. In the presence of Scand or Ridge, extremely strong SEHF is produced by a confined band of intensified meridional flux extending from the subpolar Atlantic up to Eurasian polar regions, touching the Kara Sea. Values can reach 60 K m s^{-1} in the Nordic seas and are associated with a poleward shifted and strongly tilted low-level jet in the eastern Atlantic and Europe. As noted previously, the poleward-shifted jet is typical of the Ridge regime and frequent also during Scand. This elongated pattern is slightly shifted poleward and eastward in the case of Scand, and more contracted around the Atlantic Ocean in the case of the Ridge, but essentially it can be viewed as a common mode of localized extreme SEHF in the Nordic seas that can occur in the presence of both weather regimes. Noticeable in these respects is the lack of similar zonally confined patterns for the NAO±. In this case, positive values of moderate intensity (up to 20 K m s^{-1}) are scattered over multiple sectors, from North America, to the Bering Strait, to the Barents and Kara Sseas.

The qualitative difference between the pairs Scand–Ridge and NAO± is more evident in Fig. 11: Fig. 11a shows the longitudinal profile at 70°N of the SEHF fields shown in Fig. 10. In the case of Scand–Ridge extreme flux in a zonal-mean sense is the signature of strong and localized anomalies confined in the Euro-Atlantic sector, with a peak around 0°. During NAO± the anomalous heat flux is positive over a wide area of the Northern Hemisphere, but the magnitude of anomalies over the North Atlantic is small if compared to other longitudes and values reached are locally smaller than Scand–Ridge. The bottom panel of Fig. 11 also shows that intense zonal-mean heat flux during Scand–Ridge is often found with a positive anomaly in the Euro-Atlantic domain, over a longitudinal sector that is larger than the typical size of circulation anomalies associated with regimes variability. If the extreme flux event happens during NAO± it is unlikely to find positive anomalies in the Atlantic area. This distinction does not apply to the midlatitudes, where the extreme heat flux is always associated with a distinct peak in the Atlantic, which is particularly low for NAO−.

About 7% of days during Scand and Ridge correspond to SEHF at 70°N above the 95th percentile of the total climatological distribution (i.e., including all days of the four weather regimes; see Table 1). This number drops down to about 3% for the NAO+ and NAO−. This finding implicates that more than two-thirds (69%) of the extreme SEHF days are found during Scand and Ridge, which together correspond to about 50% of days.

e. *Low-frequency heat flux*

The interest for this component is motivated by its peak in high latitudes (Fig. 1b) and by a potential association between regimes and frequency bands slightly lower than the synoptic one. The zonal mean of $V_L m_L$ and $V_L m_s + V_s m_L$ is shown in Fig. S3. The interpretation of these low-frequency terms is complicated by the lack of a dominant physical mechanism and the fact that they include the contribution of interannual variability, trends and seasonality of the occurrence of weather regimes. To investigate potential contribution from intermediate frequencies, following the rationale of Athanasiadis and Ambaum (2010) we have computed the heat flux for bandpass filtered V and m. Results for the zonal mean are

TABLE 1. Synoptic heat flux ($V_s m_s$) at 850 hPa, low-frequency heat flux ($V_L m_L + V_L m_s + V_s m_L$; HF_{LF}) at 850 hPa, and total vertically integrated heat flux ($\int V m\, dp$) for each weather regime. The left columns show the percentage of days with the given weather regimes that have zonal-mean heat flux at 70°N above the 95th-percentile threshold (computed using all days). The right columns show the percentage of days above the 95th percentile that fall in a given weather regime.

Regime	$V_s m_s$ at 850 hPa		HF_{LF} at 850 hPa		$\int V m\, dp$	
Scand	6.4	34.5	5.1	27.8	9.0	49.1
Ridge	7.8	34.9	4.2	18.8	5.9	26.5
NAO+	2.6	16.3	4.0	25.2	2.6	16.4
NAO−	3.3	11.7	7.4	26.2	2.1	7.8

shown in Fig. 12. An interesting feature of this analysis is the strong signal on the 10–30-day bands found for the NAO−: this signal is substantially larger than the 20–90-day band, peaks at a positive lag of 10 days (not shown), and is not explained by a localized peak in the Nordic seas. Indeed, the spatial structure of this signal shown in Fig. 13 reveals that the largest values are found over the Eurasian continent. There is no clear evidence of a modulation of the low-frequency heat flux explained by the terms $V_L m_L + V_s m_L + V_L m_s$ in the Nordic seas (Fig. 13) by Atlantic weather regimes for the bands considered in this study.

The analysis of heat flux extremes into the polar cap is complemented with the corresponding analysis of the lower-frequency terms and of the total heat flux. In a zonal-mean sense (see Fig. S5), the total instantaneous flux is increased in correspondence of the latitudes of anomalous meridional motion. We find that for all weather regimes interference terms are dominated by meridional advection of climatological moist static energy by the low-frequency component of the meridional velocity ($V_L m_c$). The zonal-mean heat flux at 70°N is particularly strong for Scand and for the NAO−, consistent with the strong meridional component of the geostrophic wind at that latitude (see Fig. 2) that overlaps strong zonal asymmetries of moist static energy.

Considering now synoptic heat flux extremes, the fraction of the anomalous synoptic heat flux and the corresponding regime total heat flux at 850 hPa, 70°N during these events is 0.15 for Scand and about 0.30 for the other regimes (0.28 for Ridge, 0.35 for NAO+, and 0.33 for NAO−). This fact is consistent with the strong contribution by inteference terms implied by Fig. S5. When total heat flux extremes are considered, the role of Scand stands out as about half of the days with extreme positive flux are found during this regime (Table 1). The relative contribution by lower-frequency terms ($V_L m_L + V_s m_L + V_L m_s$) is negligible, being lower than 5% for all regimes.

As indicated by Table 1, also the occurrence of extremely strong low-frequency heat flux is only weakly associated with individual regimes, and shows that the NAO− is typically associated with higher values.

4. Discussion

The analysis presented in this study reveals many features of the link between large-scale circulation regimes in the midlatitude North Atlantic and poleward heat flux by synoptic eddies. The magnitude of the synoptic heat flux within the Atlantic storm track increases with the latitude of the Atlantic jet and collapses when the jet collapses (Figs. 3 and 5h). It is remarkable that the latitude of the Atlantic jet does not capture a large variability of the high-latitude SEHF with the exception of an extremely poleward-shifted jet (Fig. 5d). Little is known about these extreme states of the jet but they may be a nonnegligible feature of the energy exchange between middle and high latitudes. There is evidence of two slightly different spatial configurations that contribute to these extremes states (see Fig. 10), one attributable to Scand and the other to Ridge. On the other hand the jet speed shows a strong correlation with the high-latitude SEHF, indicating that the disruption of the zonal flow by meridional motion, or the *waviness* of the jet, is strongly correlated with the magnitude of the high-latitude synoptic heat flux. A promising exercise could investigate the relationship between global indices of jet waviness and zonal-mean transient heat flux into the polar cap.

The interpretation of heat transport variability on synoptic time scales relies on the strong link with baroclinic instability and with the propagation of extratropical storms and their energy exchange with the mean flow. The idea of preferred transitions between regimes has been examined in previous studies (Franzke et al. 2011; Luo et al. 2012a,b). These studies describe also a preferred transition from a jet close to its mean state (essentially the NAO+), to a poleward displaced jet (JLI > 50°N, typically associated with Ridge or Scand). The state with a poleward displaced jet is preceded by the intensification of the midlatitude heat flux [Fig. 8 herein; see also Fig. 9 in Novak et al. (2015)]. The role of synoptic heat flux as a tracer of energy transfer is then attributable to the midlatitude component found in Figs. 4a, 5h, 7, and 8a. The most poleward-displaced stage of this cycle is coincident with whiffs of heat flux on synoptic frequencies (Figs. 4b,c, 5d, and 7) that typically follow the established circulation regime (Fig. 8). The skewness increasing with latitude (Fig. 9) complements the picture, indicating that for polar heat flux the relative importance of strong isolated events is larger compared

to midlatitudes, where the combination of temporally confined pulses could be a frequent phenomenon (see, e.g., Novak et al. 2015).

An intriguing fact is that the collapse of the synoptic heat flux and of the jet latitude (the NAO−) is associated with a strong flux at lower-frequency bands. The NAO− is the regime with the largest persistence in our results [not shown, but see also Faranda et al. (2017)] and projects significantly on variability patterns at longer time scales (Feldstein 2003). The picture we find is consistent the slow evolution evolution of the NAO discussed by Bollasina and Messori (2018) and could be part of the decay of the negative NAO described by Feldstein (2003). The signal found for low-frequency bands in Figs. 12 and 13 could be related to persistent NAO− associated also with tropical influence (Cassou 2008; Baggett and Lee 2015). It is important to recognize in this context the complex and multiscale nature of transport (Lembo et al. 2019) and eddy feedbacks on the mean flow (Boljka and Shepherd 2020).

A fascinating picture of blocking emerges: Fig. 7b evokes visually the steering effect of blocking on the storm path, so that blocking on the poleward (equatorward) side of the tilted Atlantic jet pushes the storm track equatorward (poleward) in a latitude band that depends on the longitude where blocking occurs. From the perspective of flow regimes (i.e., taking into account how frequent blocking is at a certain location; Fig. 7b) upstream (Greenland) blocking interacts with SEHF in the midlatitudes, and downstream (Scandinavian) blocking interacts with SEHF in the polar regions.

A dual behavior of zonally integrated extremes of synoptic heat flux on the boundary of the polar cap emerges from Figs. 10 and 11. During the NAO+ and even more clearly during the NAO−, extremely strong zonal-mean synoptic heat flux develops in the form of a synchronized increase at several longitudinal sectors, a feature that is discussed by Messori and Czaja (2015) as a possible behavior of extremes of zonally integrated transient eddy heat flux in the midlatitudes. Another possibility is that the extreme synoptic heat flux during NAO± is achieved via zonally confined pulses that are equally likely in several regions. Conversely, during Scand and Ridge, the strong flux is achieved by the local intensification in the Nordic seas. This duality is not found in the midlatitudes (Fig. 11).

An evocative perspective is to combine the concept of a local effect of synoptic disturbances (Ambaum and Novak 2014) with the nature of strong zonal-mean transient eddy transport scattered in pulses at different latitudes (Messori et al. 2017), through the idea that the transient synoptic flux happens at latitudes "selected" by a certain local flow regime. Low-frequency regimes on a large but not hemispheric scale affect the transient heat flux locally (Fig. 1) but modulate significantly (on average) the zonal-mean heat flux at all latitudes between 30° and 80°N (Fig. 4). The modulation is confined in bands of about 10°–15°.

If all the anomalous moist static energy is converted into internal energy (in the limit of no heat exchanges with Earth's surface and by radiation), then the order of magnitude of the temperature tendency explained by the synoptic heat flux modulation in Figs. 3 and 4 is about $0.1\,\mathrm{K\,day^{-1}}$ for the polar cap poleward of 70°N. In the midlatitudes this term is small compared to the associated interference term (e.g., $v'm_c \simeq v_L m_c$; see Fig. S5). It is found that the constructive contribution of synoptic and interference term is particularly effective during Scand, suggesting an important role for this regime for the climate of the Arctic. In general, on time scales of days or weeks, the tendency is dominated by the anomalous advection of climatological moist static energy and moreover the surface temperature variability is not strictly associated with the variability of meridional heat transport in the atmospheric column (Papritz 2020). Nonetheless, it is noticeable that in the pole, in particular in the high Arctic, the relative importance of the synoptic component is larger compared to midlatitudes, in a decomposition based on Atlantic regimes. In a steady state, if we associate the flux with a reference layer of 500 hPa, the modulation of the heat flux convergence by Atlantic flow regimes can explain a surface heat flux variability of about $5\,\mathrm{W\,m^{-2}}$ for the cap poleward of 70°N. This fact suggests that the steering of storms and the secundary storm activity induced by specific states of the low-frequency atmospheric variability modulate high-latitude synoptic heat flux by an amount that is relevant to the budget of the atmospheric polar cap, and thus to the exchange of heat between the atmosphere and other components of the polar cap.

The investigation presented here shows simple empirical relationships between synoptic eddy heat flux and flow regimes of the atmospheric circulation. These relationships can then be applied to coupled or uncoupled atmospheric general circulation models simulations, providing insight into model behavior and potentially improving our understanding of systematic model errors in high-latitude regions. The modulation of the synoptic flux may play a role in a (more complex) relationship between underestimation of blocking (Scaife et al. 2010) and cold bias in the Arctic (de Boer et al. 2012; Chapman and Walsh 2007).

As noted already in the introduction, transient eddy heat flux in a geophysical fluid is relevant also to the potential vorticity budget. The rationale and theoretical framework discussed in detail by Lau and Holopainen (1984) are insightful in these respects. The covariability of heat flux and wind is then to be interpreted

considering their mutual two-way interaction, as is done for instance in dynamical models of annular modes or jet regimes. A recent example is provided by the analytical model developed by Molteni and Kucharski (2019).

5. Summary

In this study the covariability between transient eddy heat flux and low-frequency weather regimes in the Atlantic regions has been examined. For high latitudes, we find that the zonal-mean synoptic heat flux is 1) intensified during Scand (at about 70°–80°N) and Ridge (at about 60°N); 2) anticorrelated with the Atlantic jet speed; 3) slightly suppressed around the climatological jet latitude and intensified when the jet latitude is very high (>55°N), being at intermediate values when the jet latitude is low (<40°N); and 4) intensified when blocking is detected over central Atlantic, British Isles, and Scandinavia. For middle latitudes the zonal-mean synoptic heat flux 1) is intensified during Ridge and NAO+ and significantly suppressed by NAO−, 2) increases linearly with jet latitude up to 60°N, then is suppressed for extremely high-latitude jet, and 3) is reduced when blocking is detected over Greenland and Iceland. Analysis of zonal-mean heat flux extremes reveals that positive extremes of high-latitude synoptic heat flux anomalies are favored by Scand and Ridge and by extreme poleward excursions of the jet latitude. More than two-thirds of the climatological transient eddy heat flux on the synoptic frequencies at 70°N is explained by the 50% of days belonging to the Scand and Ridge regimes. Similarly, the secondary storm track in the Nordic seas and the associated heat flux are modulated not by the alternating phases of the NAO, but rather by the occurrence of the Scand and/or Ridge regimes.

Acknowledgments. We are grateful to Isaac Held and two anonymous reviewers for constructive and insightful comments. The first author wishes to thank Susanna Corti and Johanna Baehr for useful discussions on an early version of the manuscript. PR was supported by the Blue-Action project (European Union's Horizon 2020 research and innovation programme, Grant 727852). MCAC was supported by the MEDSCOPE project (ERA4CS-JPI Climate with co-funding by the European Union, Grant 690462)

REFERENCES

Adams, J. M., N. A. Bond, and J. E. Overland, 2000: Regional variability of the Arctic heat budget in fall and winter. *J. Climate*, **13**, 3500–3510, https://doi.org/10.1175/1520-0442(2000)013<3500:RVOTAH>2.0.CO;2.

Ambaum, M. H. P., and L. Novak, 2014: A nonlinear oscillator describing storm track variability. *Quart. J. Roy. Meteor. Soc.*, **140**, 2680–2684, https://doi.org/10.1002/qj.2352.

Athanasiadis, P. J., and M. H. P. Ambaum, 2010: Do high-frequency eddies contribute to low-frequency teleconnection tendencies? *J. Atmos. Sci.*, **67**, 419–433, https://doi.org/10.1175/2009JAS3153.1.

Baggett, C., and S. Lee, 2015: Arctic warming induced by tropically forced tapping of available potential energy and the role of the planetary-scale waves. *J. Atmos. Sci.*, **72**, 1562–1568, https://doi.org/10.1175/JAS-D-14-0334.1.

Boljka, L., and T. G. Shepherd, 2020: Multiscale extratropical barotropic variability on the subseasonal-to-seasonal time-scale. *Quart. J. Roy. Meteor. Soc.*, **146**, 301–313, https://doi.org/10.1002/qj.3676.

Bollasina, M. A., and G. Messori, 2018: On the link between the subseasonal evolution of the North Atlantic Oscillation and East Asian climate. *Climate Dyn.*, **51**, 3537–3557, https://doi.org/10.1007/s00382-018-4095-5.

Branstator, G., 1995: Organization of storm track anomalies by recurring low-frequency circulation anomalies. *J. Atmos. Sci.*, **52**, 207–226, https://doi.org/10.1175/1520-0469(1995)052<0207:OOSTAB>2.0.CO;2.

Cassou, C., 2008: Intraseasonal interaction between the Madden–Julian Oscillation and the North Atlantic Oscillation. *Nature*, **455**, 523–527, https://doi.org/10.1038/nature07286.

Chapman, W. L., and J. E. Walsh, 2007: Simulations of Arctic temperature and pressure by global coupled models. *J. Climate*, **20**, 609–632, https://doi.org/10.1175/JCLI4026.1.

Corti, S., F. Molteni, and T. Palmer, 1999: Signature of recent climate change in frequencies of natural atmospheric circulation regimes. *Nature*, **398**, 799–802, https://doi.org/10.1038/19745.

Czaja, A., and J. Marshall, 2006: The partitioning of poleward heat transport between the atmosphere and ocean. *J. Atmos. Sci.*, **63**, 1498–1511, https://doi.org/10.1175/JAS3695.1.

de Boer, G., W. Chapman, J. E. Kay, B. Medeiros, M. D. Shupe, S. Vavrus, and J. Walsh, 2012: A characterization of the present-day Arctic atmosphere in CCSM4. *J. Climate*, **25**, 2676–2695, https://doi.org/10.1175/JCLI-D-11-00228.1.

Dee, D. P., and Coauthors, 2011: The ERA-Interim reanalysis: Configuration and performance of the data assimilation system. *Quart. J. Roy. Meteor. Soc.*, **137**, 553–597, https://doi.org/10.1002/qj.828.

Eady, E. T., 1949: Long waves and cyclone waves. *Tellus*, **1**, 33–52, https://doi.org/10.3402/tellusa.v1i3.8507.

Faranda, D., G. Messori, and P. Yiou, 2017: Dynamical proxies of North Atlantic predictability and extremes. *Sci. Rep.*, **7**, 41278, https://doi.org/10.1038/srep41278.

Feldstein, S. B., 2003: The dynamics of NAO teleconnection pattern growth and decay. *Quart. J. Roy. Meteor. Soc.*, **129**, 901–924, https://doi.org/10.1256/qj.02.76.

Franzke, C., T. Woollings, and O. Martius, 2011: Persistent circulation regimes and preferred regime transitions in the North Atlantic. *J. Atmos. Sci.*, **68**, 2809–2825, https://doi.org/10.1175/JAS-D-11-046.1.

Hannachi, A., D. M. Straus, C. L. Franzke, S. Corti, and T. Woollings, 2017: Low-frequency nonlinearity and regime behavior in the Northern Hemisphere extratropical atmosphere. *Rev. Geophys.*, **55**, 199–234, https://doi.org/10.1002/2015RG000509.

Holton, J. R., 1973: An introduction to dynamic meteorology. *Amer. J. Phys.*, **41**, 752, https://doi.org/10.1119/1.1987371.

Hoskins, B. J., I. N. James, and G. H. White, 1983: The shape, propagation and mean-flow interaction of large-scale weather

systems. *J. Atmos. Sci.*, **40**, 1595–1612, https://doi.org/10.1175/1520-0469(1983)040<1595:TSPAMF>2.0.CO;2.

Kimoto, M., and M. Ghil, 1993a: Multiple flow regimes in the Northern Hemisphere winter. Part I: Methodology and hemispheric regimes. *J. Atmos. Sci.*, **50**, 2625–2644, https://doi.org/10.1175/1520-0469(1993)050<2625:MFRITN>2.0.CO;2.

——, and ——, 1993b: Multiple flow regimes in the Northern Hemisphere winter. Part II: Sectorial regimes and preferred transitions. *J. Atmos. Sci.*, **50**, 2645–2673, https://doi.org/10.1175/1520-0469(1993)050<2645:MFRITN>2.0.CO;2.

Lau, N.-C., and E. O. Holopainen, 1984: Transient eddy forcing of the time-mean flow as identified by geopotential tendencies. *J. Atmos. Sci.*, **41**, 313–328, https://doi.org/10.1175/1520-0469(1984)041<0313:TEFOTT>2.0.CO;2.

Lembo, V., G. Messori, R. Graversen, and V. Lucarini, 2019: Spectral decomposition and extremes of atmospheric meridional energy transport in the Northern Hemisphere midlatitudes. *Geophys. Res. Lett.*, **46**, 7602–7613, https://doi.org/10.1029/2019GL082105.

Liang, M., A. Czaja, R. Graversen, and R. Tailleux, 2018: Poleward energy transport: Is the standard definition physically relevant at all time scales? *Climate Dyn.*, **50**, 1785–1797, https://doi.org/10.1007/s00382-017-3722-x.

Luo, D., J. Cha, and S. B. Feldstein, 2012a: Weather regime transitions and the interannual variability of the North Atlantic Oscillation. Part I: A likely connection. *J. Atmos. Sci.*, **69**, 2329–2346, https://doi.org/10.1175/JAS-D-11-0289.1.

——, ——, and ——, 2012b: Weather regime transitions and the interannual variability of the North Atlantic Oscillation. Part II: Dynamical processes. *J. Atmos. Sci.*, **69**, 2347–2363, https://doi.org/10.1175/JAS-D-11-0290.1.

Madonna, E., C. Li, C. M. Grams, and T. Woollings, 2017: The link between eddy-driven jet variability and weather regimes in the North Atlantic–European sector. *Quart. J. Roy. Meteor. Soc.*, **143**, 2960–2972, https://doi.org/10.1002/qj.3155.

Messori, G., and A. Czaja, 2013: On the sporadic nature of meridional heat transport by transient eddies. *Quart. J. Roy. Meteor. Soc.*, **139**, 999–1008, https://doi.org/10.1002/qj.2011.

——, and ——, 2015: On local and zonal pulses of atmospheric heat transport in reanalysis data. *Quart. J. Roy. Meteor. Soc.*, **141**, 2376–2389, https://doi.org/10.1002/qj.2529.

——, R. Geen, and A. Czaja, 2017: On the spatial and temporal variability of atmospheric heat transport in a hierarchy of models. *J. Atmos. Sci.*, **74**, 2163–2189, https://doi.org/10.1175/JAS-D-16-0360.1.

Michelangeli, P.-A., R. Vautard, and B. Legras, 1995: Weather regimes: Recurrence and quasi stationarity. *J. Atmos. Sci.*, **52**, 1237–1256, https://doi.org/10.1175/1520-0469(1995)052<1237:WRRAQS>2.0.CO;2.

Molteni, F., and F. Kucharski, 2019: A heuristic dynamical model of the North Atlantic Oscillation with a Lorenz-type chaotic attractor. *Climate Dyn.*, **52**, 6173–6193, https://doi.org/10.1007/S00382-018-4509-4.

Mullen, S. L., 1987: Transient eddy forcing of blocking flows. *J. Atmos. Sci.*, **44**, 3–22, https://doi.org/10.1175/1520-0469(1987)044<0003:TEFOBF>2.0.CO;2.

Nie, J., P. Wang, W. Yang, and B. Tan, 2008: Northern Hemisphere storm tracks in strong AO anomaly winters. *Atmos. Sci. Lett.*, **9**, 153–159, https://doi.org/10.1002/asl.186.

Novak, L., M. H. P. Ambaum, and R. Tailleux, 2015: The life cycle of the North Atlantic storm track. *J. Atmos. Sci.*, **72**, 821–833, https://doi.org/10.1175/JAS-D-14-0082.1.

Overland, J. E., P. Turet, and A. H. Oort, 1996: Regional variations of moist static energy flux into the Arctic. *J. Climate*, **9**, 54–65, https://doi.org/10.1175/1520-0442(1996)009<0054:RVOMSE>2.0.CO;2.

Papritz, L., 2020: Arctic lower-tropospheric warm and cold extremes: Horizontal and vertical transport, diabatic processes, and linkage to synoptic circulation features. *J. Climate*, **33**, 993–1016, https://doi.org/10.1175/JCLI-D-19-0638.1.

Peixoto, J. P., and A. H. Oort, 1992: *Physics of Climate*. American Institute of Physics, 520 pp.

Rivière, G., 2009: Effect of latitudinal variations in low-level baroclinicity on eddy life cycles and upper-tropospheric wave-breaking processes. *J. Atmos. Sci.*, **66**, 1569–1592, https://doi.org/10.1175/2008JAS2919.1.

Scaife, A. A., T. Woollings, J. Knight, G. Martin, and T. Hinton, 2010: Atmospheric blocking and mean biases in climate models. *J. Climate*, **23**, 6143–6152, https://doi.org/10.1175/2010JCLI3728.1.

Scherrer, S. C., M. Croci-Maspoli, C. Schwierz, and C. Appenzeller, 2006: Two-dimensional indices of atmospheric blocking and their statistical relationship with winter climate patterns in the Euro-Atlantic region. *Int. J. Climatol.*, **26**, 233–249, https://doi.org/10.1002/joc.1250.

Schulzweida, U., 2018: CDO user guide (version 1.9.3). https://doi.org/10.5281/zenodo.2558193.

Seierstad, I. A., D. B. Stephenson, and N. G. Kvamstø, 2007: How useful are teleconnection patterns for explaining variability in extratropical storminess? *Tellus*, **59A**, 170–181, https://doi.org/10.1111/j.1600-0870.2007.00226.x.

Simmons, A. J., and B. J. Hoskins, 1978: The life cycles of some nonlinear baroclinic waves. *J. Atmos. Sci.*, **35**, 414–432, https://doi.org/10.1175/1520-0469(1978)035<0414:TLCOSN>2.0.CO;2.

Straus, D. M., 2010: Synoptic-eddy feedbacks and circulation regime analysis. *Mon. Wea. Rev.*, **138**, 4026–4034, https://doi.org/10.1175/2010MWR3333.1.

Tibaldi, S., and F. Molteni, 1990: On the operational predictability of blocking. *Tellus*, **42A**, 343–365, https://doi.org/10.3402/tellusa.v42i3.11882.

Trenberth, K. E., and J. M. Caron, 2001: Estimates of meridional atmosphere and ocean heat transports. *J. Climate*, **14**, 3433–3443, https://doi.org/10.1175/1520-0442(2001)014<3433:EOMAAO>2.0.CO;2.

Watt-Meyer, O., and P. J. Kushner, 2018: Why are temperature and upward wave activity flux positively skewed in the polar stratosphere? *J. Climate*, **31**, 115–130, https://doi.org/10.1175/JCLI-D-17-0155.1.

Woods, C., R. Caballero, and G. Svensson, 2013: Large-scale circulation associated with moisture intrusions into the Arctic during winter. *Geophys. Res. Lett.*, **40**, 4717–4721, https://doi.org/10.1002/grl.50912.

Woollings, T., A. Hannachi, and B. Hoskins, 2010: Variability of the North Atlantic eddy-driven jet stream. *Quart. J. Roy. Meteor. Soc.*, **136**, 856–868, https://doi.org/10.1002/qj.625.

Yiou, P., K. Goubanova, Z. X. Li, and M. Nogaj, 2008: Weather regime dependence of extreme value statistics for summer temperature and precipitation. *Nonlinear Processes Geophys.*, **15**, 365–378, https://doi.org/10.5194/npg-15-365-2008.